# Intraoperative Imaging of Tumors Using Cerenkov Luminescence Endoscopy: A Feasibility Experimental Study

Hongguang Liu*[1], Colin M. Carpenter*[2], Han Jiang[1], Guillem Pratx[2], Conroy Sun[2], Michael P. Buchin[3], Sanjiv S. Gambhir[1,4], Lei Xing[2], and Zhen Cheng[1]

*[1]Molecular Imaging Program at Stanford (MIPS), Department of Radiology and Bio-X Program, Canary Center at Stanford for Cancer Early Detection, Stanford University, Stanford, California; [2]Department of Radiation Oncology, Stanford University, Stanford, California; [3]Stanford Photonics, Inc., Palo Alto, California; and [4]Department of Bioengineering and Materials Science and Engineering, Stanford University, Stanford, California*

Cerenkov luminescence imaging (CLI) is an emerging new molecular imaging modality that is relatively inexpensive, easy to use, and has high throughput. CLI can image clinically available PET and SPECT probes using optical instrumentation. Cerenkov luminescence endoscopy (CLE) is one of the most intriguing applications that promise potential clinical translation. We developed a prototype customized fiberscopic Cerenkov imaging system to investigate the potential in guiding minimally invasive surgical resection. **Methods:** All experiments were performed in a dark chamber. Cerenkov luminescence from $^{18}$F-FDG samples containing decaying radioactivity was transmitted through an optical fiber bundle and imaged by an intensified charge-coupled device camera. Phantoms filled with $^{18}$F-FDG were used to assess the imaging spatial resolution. Finally, mice bearing subcutaneous C6 glioma cells were injected intravenously with $^{18}$F-FDG to determine the feasibility of in vivo imaging. The tumor tissues were exposed, and CLI was performed on the mouse before and after surgical removal of the tumor using the fiber-based imaging system and compared with a commercial optical imaging system. **Results:** The sensitivity of this particular setup was approximately 45 kBq (1.21 μCi)/300 μL. The 3 smallest sets of cylindric holes in a commercial SPECT phantom were identifiable via this system, demonstrating that the system has a resolution better than 1.2 mm. Finally, the in vivo tumor imaging study demonstrated the feasibility of using CLI to guide the resection of tumor tissues. **Conclusion:** This proof-of-concept study explored the feasibility of using fiber-based CLE for the detection of tumor tissue in vivo for guided surgery. With further improvements of the imaging sensitivity and spatial resolution of the current system, CLE may have a significant application in the clinical setting in the near future.

Received Nov. 1, 2011; revision accepted May 2, 2012.

For correspondence or reprints contact either of the following: Zhen Cheng, Molecular Imaging Program at Stanford, Department of Radiology, Bio-X Program, Canary Center at Stanford for Cancer Early Detection, 1201 Welch Rd., Lucas Expansion, P095, Stanford University, Stanford, CA 94305.
E-mail: zcheng@stanford.edu
Lei Xing, Department of Radiation Oncology, Stanford University School of Medicine, 875 Blake Wilbur Dr., Stanford, CA 94305-5847.
E-mail: lei@stanford.edu
*Contributed equally to this work.

Published online Aug. 17, 2012.



**Key Words:** fiber-based imaging; Cerenkov luminescence endoscopy; Cerenkov luminescence imaging; radionuclides; optical imaging; PET

**J Nucl Med 2012; 53:1579–1584**
DOI: 10.2967/jnumed.111.098541

Cerenkov luminescence imaging (CLI) has recently attracted increasing interest in the field of molecular imaging (*1,2*). CLI is a new optical imaging modality in which images are obtained by monitoring the Cerenkov photons emitted from highly energetic moving charged particles ($\beta^+$ or $\beta^-$). Conventional nuclear imaging methods, such as PET and SPECT, are the most widely used clinical molecular imaging techniques. However, these modalities usually suffer from high cost, limited availability, relatively low spatial resolution, and low throughput (*3*). As a technique that bridges optical imaging and radionuclide imaging, CLI has shown many advantages such as high sensitivity, high resolution, low cost, wide availability, relatively high throughput, and commercially available radionuclide probes already approved by the Food and Drug Administration.

Since its discovery in 2009, CLI has quickly become a practical molecular imaging technique, and many new applications of CLI in preclinical research continue to emerge (*1,2*). Several research groups have demonstrated that CLI can be a powerful tool for tumor imaging using radionuclide probes such as $^{18}$F-FDG. Important validation studies have also been performed, and it was reported that there is a good linear correlation between the tumor uptake quantified by PET and tumor CLI signals in subcutaneous xenograft models (*4–7*). CLI has also been found to be useful for imaging α and pure $\beta^-$ emitters such as $^{90}$Y and $^{225}$Ac, which are used for cancer treatment (*4*). Moreover, CLI can be applied in the monitoring of reporter gene expression. The herpes simplex virus type 1 thymidine kinase and the sodium iodide symporter reporter genes were recently successfully imaged by CLI in conjunction with

appropriate radioactive reporter probes (*4,8,9*). Cerenkov photons have also been used to illuminate fluorescent dyes and nanoparticles for in vivo imaging (*10–13*). A recent study further showed that CLI could be used for monitoring tumor surgery in xenograft mouse models, highlighting the translational potential of the modality (*14*). CLI has also been used to measure the radiochemical purity of a radiolabeled compound and to image plant physiology (*15*). In addition to these applications, the recent advancement in CLI tomography makes this novel imaging modality even more powerful and promising for biomedical research including diagnostic imaging and therapeutic monitoring (*16–19*).

Because it can image clinically available radiotracers, CLI has the potential to be rapidly translated into clinical applications (*4,18*). However, all the studies described above have involved the use of conventional small-animal optical imaging systems, which are not compatible with routine clinical practice. In this study, we have built the first, to our knowledge, prototype system that is amenable to Cerenkov luminescence endoscopy (CLE) in the clinic. This system comprises an optical fiber bundle and an intensified charge-coupled device (CCD) camera. The small-diameter flexible endoscope is designed for minimally invasive monitoring of living tissues and organs, using a sensitive camera to produce images of the radionuclide probe. It is also expected that hollow organs (e.g., bladder and lung) or insufflated cavities (e.g., esophagus and colon) inside the body can provide natural and anatomic dark chambers for CLE. By overlaying conventional bright-field images commonly obtained from an endoscope with the Cerenkov luminescence images generated by radionuclide probes, CLE could be used to identify diseased tissues for diagnostic purposes and real-time monitoring of endoscopic surgery.

Therefore, we investigated the feasibility of CLE for guiding cancer surgical resection by performing sensitivity, spatial-resolution, and proof-of-concept experiments. The characteristic sensitivity of this system was evaluated using the natural decay of $^{18}$F-FDG. Imaging resolution was determined using a phantom with cylindric holes. Finally, imaging studies were performed to demonstrate surgical guidance in a small-animal tumor model. A well-known commercial optical imaging system was used to provide a comparison. The data presented herein outline the instrumentation and methodology; further steps that are needed to translate this modality into the clinic are also discussed.

## MATERIALS AND METHODS

$^{18}$F-FDG was produced by the Radiochemistry Facility at Stanford University. The rat glioma cell line C6 was obtained from American Type Culture Collection. Female athymic nude mice (*nu/nu*) ($n = 5$) obtained from Charles River Laboratories, Inc., were 4–6 wk old. A CRC-15R PET dose calibrator (Capintec Inc.) was used for all radioactivity measurements.

### Tumor Model

All animal studies were performed in compliance with federal and local institutional guidelines for the conduct of animal experimentation. C6 cells were cultured in Dulbecco modified Eagle medium supplemented with 10% fetal bovine serum and 1% penicillin/streptomycin (Invitrogen Life Technologies). The cell line was maintained in a humidified atmosphere of 5% $CO_2$ at 37°C, with the medium changed every other day. A 75% confluent monolayer was detached with trypsin and dissociated into a single-cell suspension for further cell culture. Approximately $1 \times 10^6$ C6 cells suspended in phosphate-buffered saline (0.1 M, pH 7.2; Invitrogen) were implanted subcutaneously in the left legs of nude mice. Tumors were allowed to grow to 150–200 mm$^3$ (2–3 wk), and the tumor-bearing mice were imaged in vivo.

### CLI

Validation CLI was performed with an IVIS Spectrum system (Caliper Life Sciences). For all in vivo studies, radionuclides were diluted in phosphate-buffered saline. Animals were placed in a light-tight chamber under isoflurane anesthesia. Each acquisition took 3 min for all studies without filters. Images were acquired and analyzed using Living Image 3.0 software (Caliper Life Sciences). The mice were kept fasting overnight before $^{18}$F-FDG imaging and anesthetized by inhalation of 2% isoflurane during the experiment.

### Fiber-Based CLE System

The fiber-based CLE system used an imaging optical fiber coupled to a highly sensitive intensified CCD camera. The application of this system for surgical oncology guidance is detailed in Figure 1. Specifically, a microimaging lens (Cinegon, F/1.4, 12-mm focal length; Schneider) was coupled at the distal end of an optical imaging fiber bundle that was 108 mm long, with a $5 \times 6.7$ mm active area. The pixels of the fiber bundle are made of discrete 10-μm fibers (IG154; Schott). At the proximal end, a Pentax (F/1.4) lens provided relay optics to the camera (Supplemental Fig. 1A; supplemental materials are available online only at http://jnm.snmjournals.org). The camera, an image-intensified

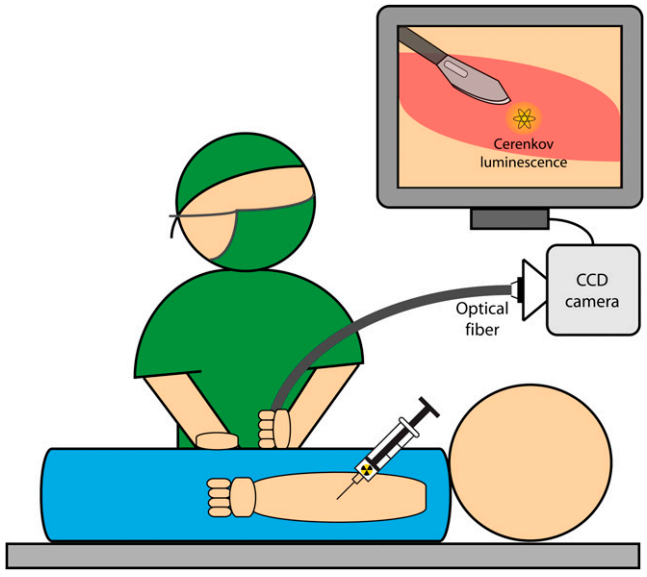


**FIGURE 1.** Suggested application of fiber-based system for endoscopic and laparoscopic CLI.

CCD (Turbo 640-Z; Stanford Photonics Inc.), had 640 × 480 pixels and single-photon imaging capability (Supplemental Fig. 1B). To minimize background light and to emulate a light-tight anatomic cavity, all images were taken in a dark box. In addition, images were postprocessed with a software thresholding technique that removed pixel values below a manufacturer-recommended value; this optimal value was chosen to remove low-intensity pixels that corresponded to thermal and read noise on the CCD. These steps reduced the noise to approximately 20 counts per second.

### Imaging Using Fiber-Based System

Images were acquired at a high frame-rate of 120 Hz to allow for maximal reduction in noise. The noise-reduction step described above was performed for each frame. These frames were then accumulated for 5 min to form the raw data. The raw data were image-processed offline using an algorithm to remove cosmic and stray γ-events. This algorithm removed noisy pixels by thresholding the gradient around each pixel in its local area. An additional denoising step removed spurious bright pixels that appeared in sequential exposures.

The fiber-based CLE system was characterized for sensitivity by imaging 2 adjacent wells of a black 96-well plate (300 μL per well). A glycerol and water mixture combined with 3.7 MBq (100 μCi) of $^{18}$F-FDG was in 1 well, and a glycerol and water mixture only was in a nearby well. Images were sequentially acquired over approximately 10 half-lives (19 h, 43 min), and each data point was formed from 5 min of photon accumulation.

The spatial resolution of the system was characterized using a standard PET/SPECT phantom (Micro Hot-Spot Phantom; Data Spectrum Corp.) filled with 15.2 MBq (410 μCi) of $^{18}$F-FDG; this phantom is also commonly used to evaluate the spatial resolution of PET systems. Both the 2.4- and the 1.6-mm cylindric holes were used to form line profiles, taken from the fiber-based images. An ambient-light image and a functional Cerenkov luminescence image were acquired. The exposure time for all ambient images was less than 1 s, and the functional image acquisition time was 5 min. The subject was 5 cm from the optical system.

### Fiber-Based CLE System for Surgery Monitoring

Five mice were injected with 37 MBq (1 mCi) of $^{18}$F-FDG via the tail vein. The tracer was allowed to accumulate for 60–70 min, and the mice were imaged in the IVIS system to verify tumor uptake of $^{18}$F-FDG. Tumors were then imaged with the IVIS and fiber-based CLE systems after removal of the skin covering the subcutaneous tumor and after excision of the tumor. To simulate an environment mimicking surgical resection, and to validate the origin of the signal, the excised tumor was also imaged after being placed adjacent to the surgical cavity. Two images were acquired for each of these steps: 1 ambient image and 1 functional Cerenkov luminescence image. The exposure time for all ambient images was less than 1 s, and the functional image acquisition time was 5 min.

### Statistical Methods

Quantitative data were expressed as mean ± SD. Means were compared using the Student *t* test. A 95% confidence level was chosen to determine the significance between groups, with *P* values of less than 0.05 indicating significant differences.

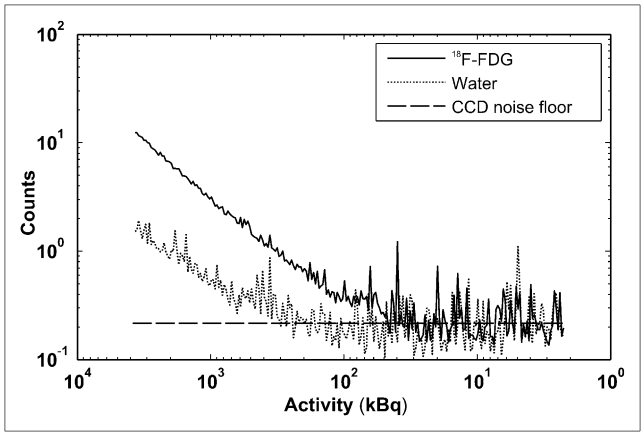


**FIGURE 2.** System sensitivity via sequential imaging of 3.7 MBq (100 μCi) of $^{18}$F-FDG for approximately 20 h. Optical signals from $^{18}$F-FDG and control sample were plotted.

## RESULTS

### System Characterization

Figure 2 shows the reduction in signal during $^{18}$F-FDG decay over time for 2 wells: 1 filled with $^{18}$F-FDG and 1 filled with a water and glycerol mixture only. With a 5-min integration time, a minimum of approximately 45 kBq (1.21 μCi) of activity can be identified as different from the control well containing the water and glycerol solution (signal-to-noise ratio $> 1$). There was a decrease in signal in the control well due to stray γ-photons from the $^{18}$F-FDG well interacting with the optical fiber and creating scintillation background light in the image.

Visually, the photographic and Cerenkov images taken using the standard IVIS imaging system (Supplemental Fig. 2) are similar to the photographic and Cerenkov images taken with the fiber-based system (Fig. 3A). The line profiles demonstrate a high correlation between the Cerenkov and photographic line profiles. For the 2.4-mm holes (Fig. 3B), the line profile limits depicted by the large green stars in Figure 3A had a Pearson correlation coefficient of 0.78 (significance, $P < 1e{-}5$). For the 1.6-mm holes (Supplemental Fig. 3), the line profile limits depicted by the smaller red stars had a Pearson correlation coefficient of 0.71 (significance, $P < 1e{-}5$). The peaks were also in near-identical locations; the difference in peak locations between the holes for the line profiles of the photographic and Cerenkov-emission images was 3.8%, a difference of only a few pixels.

### System Demonstration

The images comparing both systems before removal of the tumor for mouse 1 are shown in Figure 4 (IVIS system [Fig. 4A] and fiber-based CLE system [Fig. 4B]). Figure 5A shows the images produced by the IVIS system, and Figure 5B shows images from the fiber-based CLE system after removal of the tumor in mouse 1.

Comparing images in Figure 5B quantitatively, we determined the tumor-to-background ratio for the Cerenkov signal by computing the ratio of the median value in the

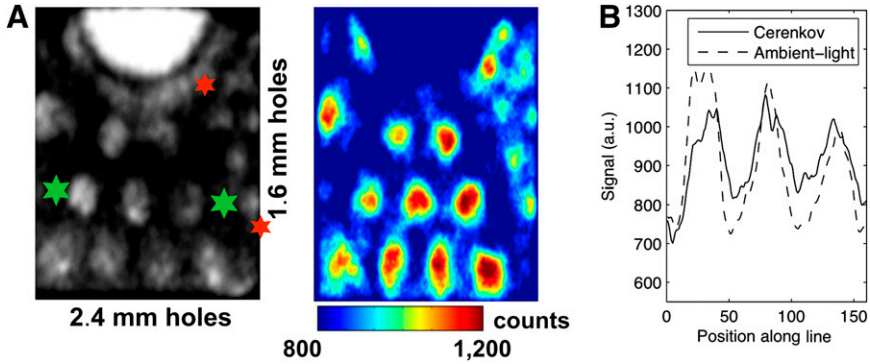


**FIGURE 3.** Characterization of fiberscopic system spatial resolution. (A) Respective ambient (left) and Cerenkov images (right) of PET/SPECT phantom (4.3-cm inner diameter). (B) Quantitative line profiles of ambient and Cerenkov images for 2.4-mm holes; line sampled is indicated by green stars in A. a.u. = arbitrary units.

region of interest encircling the excised tumor to the median value in the cleared tumor cavity. This ratio was 1.28 (for comparison, the tumor-to-background ratio from the IVIS system was 1.16 for the 3-min scan). For mice 2, 3, 4, and 5, the tumor-to-background ratios for the removed tumor were 1.41, 1.21, 1.02, and 1.17, respectively. Tumor tissue light emission was significantly higher than the exposed cavity for all mice (Student *t* test for paired samples, $P < 0.05$ for all). Much of the low tumor-to-background value in mouse 4 can be explained by the reflection of the light emitted from the tumor by the tumor cavity, which was directly adjacent. Residual tumor tissue after surgery is also possible.

## DISCUSSION

In this study, we demonstrated the methodology and performance of an optical fiber system built to image tumor margins during surgical resection. Cerenkov imaging has been proposed for small-animal drug discovery and surgical guidance, yet previous studies have used an imaging box with a lens-mounted imaging system; this setup is not realistic for subjects that are larger (e.g., large animals and humans). We recently demonstrated the feasibility of endoscopic imaging of Cerenkov light using conventional optical fiber bundle/clinical endoscopes, an optical imaging lens system, and a sensitive low-noise CCD camera (*20*). Hereby, for the first time we investigated a Cerenkov endoscope for surgical resection. We have shown that this system is capable of imaging 1.2-mm structures, using phantom experiments. We determined the sensitivity of the system for $^{18}$F-FDG (~45 kBq [1.21 μCi]/300 μL). We then demonstrated the ability to visualize the accumulation of $^{18}$F-FDG in a tumor using this system and could track the contrast as the tumor was excised from the mouse.

A benefit of a Cerenkov endoscope is that it provides higher image spatial resolution than PET and SPECT cameras, because the optical photons emitted from the tissue surface are detected with optical lenses and a high-resolution CCD chip. Cho et al. demonstrated a limit of 350 μm (in full width at half maximum) with a system designed for visualizing a microfluidic chip setup (*21*). This resolution is affected by the imaging system, the range of the β-particles in the tissue, and tissue optical scatter. Levin and Hoffman showed that the mean β-particle track of $^{18}$F-FDG had a full width at half maximum value of 102 μm in water (*22*), which determines the physical resolution limit of a Cerenkov scope when imaging $^{18}$F-FDG. Improved resolution may be achieved using a radioisotope with a β-particle decay of lower energy, such as $^{131}$I, although this would result in lower sensitivity because there is an inverse relationship between resolution and sensitivity. We do note some inconsistency in the image of the 1.2-mm holes, but many of these holes are clearly visualized. The high spatial resolution of the system requires accurate focus of the optics both at the distal fiber–lens junction and at the proximal fiber–camera junction—an optical focus that will be improved in our further

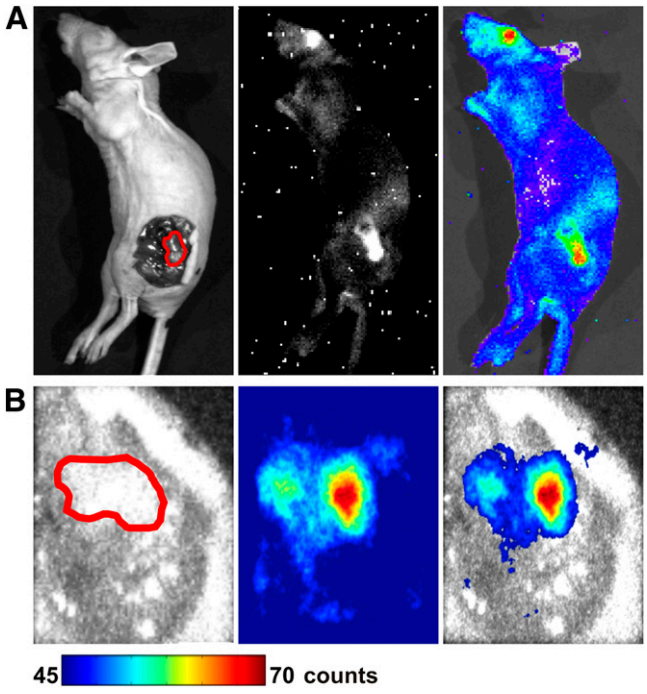


**FIGURE 4.** Mouse 1 bearing C6 glioma after tail-vein administration of 37 MBq (1 mCi) of $^{18}$F-FDG. (A) Mouse was imaged by commercially available optical IVIS system, and images were compared with those from prototype fiber-based system (B). Tumor tissues are outlined by red lines. Ambient-light images are on left, luminescent images are in middle, and fused images are on right.

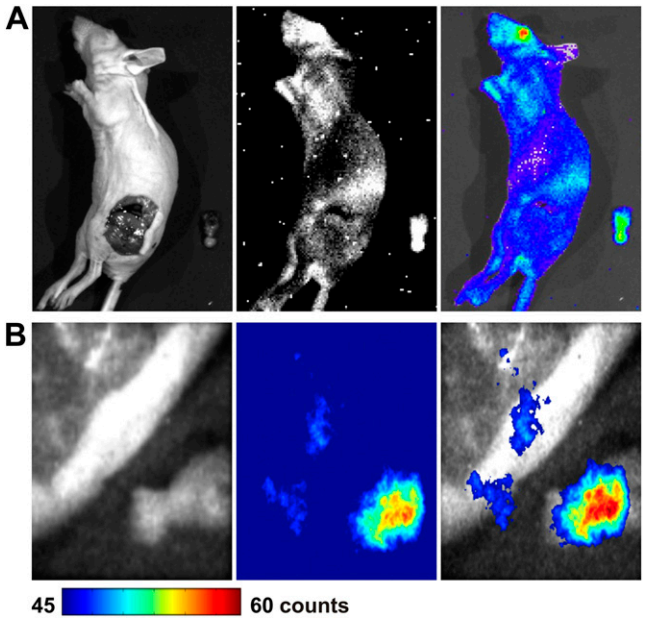


**FIGURE 5.** Mouse 1 was imaged by IVIS optical system (A) and fiber-based system (B) after surgery to remove tumor tissues. Ambient-light images are on left, luminescent images are in middle, and fused images are on right.

studies. In the case of our phantom, the resolution of the Cerenkov luminescence images was also degraded by reflections within the translucent phantom and the signal-to-noise ratio of the single-photon–counting camera, which was not entirely optimized. The signal-to-noise ratio of our ambient-light image was also affected by a slightly imperfect focus and the suboptimal settings of the illumination source and camera. Thus, although we demonstrated the ability to visualize many of these 1.2-mm cylindric holes in a phantom with this endoscope-based system, we expect to be able to image submillimeter lesions with a more optimized system.

The sensitivity limit of this system was 45 kBq (1.2 μCi)/300 μL with $^{18}$F-FDG. To put this in a practical perspective, if this system were used for head and neck tumors of the oropharynx (with a standardized uptake value of 5.17), 2.1 GBq (54 mCi) would have to be injected intravenously into a 70-kg patient to have enough activity to visualize a 300-μg tumor (*23*) in a 5-min scan; a more sensitive scope would enable the identification of smaller structures or similar structures with a reduction in ionizing dose to the patient and clinical staff. Increased sensitivity may be realized with more sensitive optics (such as an F/0.95 lens) or fiber optic glass, which transmits farther into the violet and ultraviolet emissions. The fiberglass used in this experiment was Schott-75 glass, which transmits 40% light at 500 nm; thus, it is not optimized for detecting the short-wavelength–dominant Cerenkov emission. In addition, γ-photons emitted from the radiotracer scintillate impurities in the glass, resulting in undesired background noise. The use of fused silica, which is much more sensitive to the ultraviolet and violet emissions and has fewer impurities, would improve sensitivity.

As a prototype device, the off-the-shelf optical lens on this system was too large (3-cm diameter) for many endoscopic or laparoscopic applications. However, smaller custom optics could be designed to enable imaging through smaller apertures. Meanwhile, optimized optic lenses and fibers can provide better sensitivity and shorter integration time in upcoming systems. We leave this investigation for future studies using more customized optical systems.

The main advantage of this system over other optical techniques, such as fluorescence imaging, is that it is able to use standard PET tracers, such as $^{18}$F-FDG, which are already available in the clinic. Many novel tracers such as 3′-deoxy-3′-$^{18}$F-fluorothymidine, engineered proteins, and labeled arginine-glycine-aspartic acid peptides are in the pipeline of clinical trials required by the Food and Drug Administration because of their utility in PET. This is a significant advantage for this technique, because much effort and innovation is being dedicated to PET tracers. In contrast, because of the lack of a standardized imaging device for optical imaging, optical contrast agents are not being sufficiently developed to keep pace with radiotracers. Thus, the main advantage of a Cerenkov emission surgical scope is that it is readily clinically translatable. The combination of PET and Cerenkov imaging provides an opportunity to use an identical signal origin, and perhaps an identical injection, to localize tumors for excision.

## CONCLUSION

This proof-of-concept study demonstrated the feasibility of using fiber-based CLE for the detection of tumor tissue in vivo and demonstrated its potential use for image-guided surgery. With further improvement in imaging sensitivity and resolution of the current system, it is expected that Cerenkov imaging might soon be translated into clinical applications.

## DISCLOSURE STATEMENT

The costs of publication of this article were defrayed in part by the payment of page charges. Therefore, and solely to indicate this fact, this article is hereby marked "advertisement" in accordance with 18 USC section 1734.

## ACKNOWLEDGMENTS

We acknowledge support from the National Cancer Institute (NCI) (R01 CA128908), the National Institutes of Health (ICMIC P50CA114747), the Department of Defense Breast Cancer Postdoctoral Fellowship (W81XWH-11-1-0087, W81XWH-11-1-0070, and W81XWH-10-1-0506), the Center for Biomedical Imaging at Stanford, the Canary Foundation, and the Friends for an Earlier Breast Cancer Test. No other potential conflict of interest relevant to this article was reported.

## REFERENCES


1. Xu Y, Liu H, Cheng Z. Harnessing the power of radionuclides for optical imaging: Cerenkov luminescence imaging. *J Nucl Med.* 2011;52:2009–2018.
2. Lucignani G. Cerenkov radioactive optical imaging: a promising new strategy. *Eur J Nucl Med Mol Imaging.* 2011;38:592–595.
3. Massoud TF, Gambhir SS. Molecular imaging in living subjects: seeing fundamental biological processes in a new light. *Genes Dev.* 2003;17:545–580.
4. Liu H, Ren G, Miao Z, et al. Molecular optical imaging with radioactive probes. *PLoS ONE.* 2010;5:e9470.
5. Robertson R, Germanos MS, Li C, Mitchell GS, Cherry SR, Silva MD. Optical imaging of Cerenkov light generation from positron-emitting radiotracers. *Phys Med Biol.* 2009;54:N355-365.
6. Boschi F, Calderan L, D'Ambrosio D, et al. In vivo $^{18}$F-FDG tumour uptake measurements in small animals using Cerenkov radiation. *Eur J Nucl Med Mol Imaging.* 2011;38:120–127.
7. Ruggiero A, Holland JP, Lewis JS, Grimm J. Cerenkov luminescence imaging of medical isotopes. *J Nucl Med.* 2010;51:1123–1130.
8. Liu H, Ren G, Liu S, et al. Optical imaging of reporter gene expression using a positron-emission-tomography probe. *J Biomed Opt.* 2010;15:060505.
9. Jeong SY, Hwang MH, Kim JE, et al. Combined Cerenkov luminescence and nuclear imaging of radioiodine in the thyroid gland and thyroid cancer cells expressing sodium iodide symporter: initial feasibility study. *Endocr J.* 2011; 58:575–583.
10. Liu H, Zhang XF, Xing BG, Han PZ, Gambhir SS, Cheng Z. Radiation-luminescence-excited quantum dots for in vivo multiplexed optical imaging. *Small.* 2010;6:1087–1091.
11. Dothager RS, Goiffon RJ, Jackson E, Harpstrite S, Piwnica-Worms D. Cerenkov radiation energy transfer (CRET) imaging: a novel method for optical imaging of PET isotopes in biological systems. *PLoS ONE.* 2010;5:e13300.
12. Lewis MA, Kodibagkar VD, Oz OK, Mason RP. On the potential for molecular imaging with Cerenkov luminescence. *Opt Lett.* 2010;35:3889–3891.
13. Sun C, Pratx G, Carpenter CM, et al. Synthesis and radioluminescence of PEGylated Eu(3+)-doped nanophosphors as bioimaging probes. *Adv Mater.* 2011;23:H195–H199.
14. Holland JP, Normand G, Ruggiero A, Lewis JS, Grimm J. Intraoperative imaging of positron emission tomographic radiotracers using Cerenkov luminescence emissions. *Mol Imaging.* 2011;10:177–186.
15. Park JC, An GI, Park SI, et al. Luminescence imaging using radionuclides: a potential application in molecular imaging. *Nucl Med Biol.* 2011;38:321–329.
16. Hu Z, Liang J, Yang W, et al. Experimental Cerenkov luminescence tomography of the mouse model with SPECT imaging validation. *Opt Express.* 2010;18:24441–24450.
17. Li C, Mitchell GS, Cherry SR. Cerenkov luminescence tomography for small-animal imaging. *Opt Lett.* 2010;35:1109–1111.
18. Spinelli AE, Kuo C, Rice BW, et al. Multispectral Cerenkov luminescence tomography for small animal optical imaging. *Opt Express.* 2011;19:12605–12618.
19. Xu Y, Chang E, Liu H, Jiang H, Gambhir SS, Cheng Z. Proof-of-concept study of monitoring cancer drug therapy with Cerenkov luminescence imaging. *J Nucl Med.* 2012;53:312–317.
20. Kothapalli SR, Liu H, Liao JC, Cheng Z, Gambhir SS. Endoscopic imaging of Cerenkov luminescence. *Biomed Opt Express*. 2012;3:1215–1225.
21. Cho JS, Taschereau R, Olma S, et al. Cerenkov radiation imaging as a method for quantitative measurements of beta particles in a microfluidic chip. *Phys Med Biol.* 2009;54:6757–6771.
22. Levin CS, Hoffman EJ. Calculation of positron range and its effect on the fundamental limit of positron emission tomography system spatial resolution. *Phys Med Biol.* 1999;44:781–799.
23. Allal AS, Slosman DO, Kebdani T, Allaoua M, Lehmann W, Dulguerov P. Prediction of outcome in head-and-neck cancer patients using the standardized uptake value of 2-[18f]fluoro-2-deoxy-d-glucose. *Int J Radiat Oncol Biol Phys.* 2004;59:1295–1300.